Click Here for Full Article

TRMM-TMI satellite observed soil moisture and vegetation density (1998–2005) show strong connection with El Niño in eastern Australia

Yi Liu,[1,2] Richard A. M. de Jeu,[1] Albert I. J. M. van Dijk,[2] and Manfred Owe[3]

Received 7 April 2007; revised 24 May 2007; accepted 5 July 2007; published 4 August 2007.

[1] Spatiotemporal patterns in soil moisture and vegetation water content across mainland Australia were investigated from 1998 through 2005, using TRMM/TMI passive microwave observations. The Empirical Orthogonal Function technique was used to extract dominant spatial and temporal patterns in retrieved estimates of moisture content for the top 1-cm of soil (θ) and vegetation moisture content (via optical depth τ). The dominant temporal θ and τ patterns were strongly correlated to the El Niño Southern Oscillation Index (SOI) in spring (r^2 = 0.90), and to a progressively lesser extent autumn, summer and winter. The Indian Ocean Dipole (IOD) index also explained part of the variation in spring θ and τ. Correlation analysis suggested that the regions most affected by El Niño are mainly located in eastern Australia. The results suggest that the drought conditions experienced in eastern Australia since 2000 and clearly expressed in these satellite observations have a strong connection with El Niño. **Citation:** Liu, Y., R. A. M. de Jeu, A. I. J. M. van Dijk, and M. Owe (2007), TRMM-TMI satellite observed soil moisture and vegetation density (1998–2005) show strong connection with El Niño in eastern Australia, *Geophys. Res. Lett.*, *34*, L15401, doi:10.1029/2007GL030311.

1. Introduction

[2] Australia is subject to frequent droughts, resulting in significant impact on the economy and environment [*Horridge et al.*, 2005]. Inter-decadal phases of wetter and drier conditions are observed in rainfall records [*Beeton et al.*, 2006]. Many areas have been experiencing extraordinary drought conditions since 2000. There are questions about the possible causes of this drought: an extreme event, natural climate cycling, and/or a consequence of human-induced climate change. Rainfall patterns have been linked to several ocean circulation indicators: droughts to sea surface temperature anomalies (SSTA) over the eastern Indian Ocean [*Streten*, 1981, 1983]; winter rainfall patterns in western and southern Australia to the Indian Ocean Dipole (IOD) [*Ashok et al.*, 2003]; southeastern Queensland rainfall to central Pacific Ocean SSTA [*Murphy and Ribbe*, 2004]; and the 2001/02 drought to a modest El Niño event [*Nicholls*, 2004]. Spatial patterns, interactions, and changes in the connection between rainfall and different aspects of ocean circulation need to be better understood [*Abram et al.*, 2007] to put the current drought in appropriate context and allow statements about future drought frequency and severity to be made with greater confidence.

[3] Soil moisture and vegetation conditions are strong indicators of antecedent weather conditions, ecosystem state and drought [*McVicar and Jupp*, 1998]. They can be inferred from satellite observations, by making use of the spectrally distinct behavior of chlorophyll in green canopies in the visible and near infrared wavebands [*Campbell*, 2002] and/or that of water in biomass and top soil in the near to thermal infrared and microwave spectra [*Choudhury*, 1993; *Fensholt and Sandholt*, 2003; *McVicar and Jupp*, 2002]. Observations of passive microwave emissions have certain advantages, in that: (1) they are available regardless of cloud cover; (2) there is a physical relationship relating emissions to water amounts in the environment; and (3) rather than the land surface only, they provide information on water content of the top soil layer (albeit still only a few cm deep). Potential disadvantages are the coarse resolution of observation (>10 km) and the lack of a consistent and continuous observation program over the past decades. A recently developed approach to retrieving surface parameters from microwave emissions can be used for all bands in the microwave domain [*de Jeu and Owe*, 2003; *Owe et al.*, 2001; *Wagner et al.*, 2007; *Owe et al.*, 2007], allowing data collected by different satellites since 1978 to yield a time series covering 30 years.

[4] As a first step in determining the potential use of such a longer time series, we explored the link between three ocean circulation indicators and spatiotemporal patterns in soil moisture and vegetation condition for an 8-year data set of passive microwave derived soil moisture and vegetation condition recently developed by *Owe et al.* [2007].

2. Data and Methods

2.1. Data

[5] The Microwave Instrument (TMI) on board NASA's Tropical Rainfall Measuring Mission (TRMM) has provided operational passive microwave measurements at 10.7 GHz (X-band) and eight higher frequencies including the 37 GHz (Ka) band since December 1997 [*Kummerow et al.*, 1998]. The observations can be assimilated in a microwave radiation transfer model to infer soil moisture, and a set of atmospheric, soil and vegetation variables, including soil and canopy temperature and vegetation optical depth.

[6] We used the top soil moisture content (θ in $m^3\ m^{-3}$) retrieved using the Land Parameter Retrieval Model (LPRM) [*Owe et al.*, 2001; *de Jeu and Owe*, 2003;

[1]Department of Hydrology and Geo-Environmental Sciences, Faculty of Earth and Life Sciences, Vrije Universiteit, Amsterdam, Netherlands.
[2]Commonwealth Scientific and Industrial Research Organization, Division of Land and Water, Black Mountain Laboratory, Canberra, A.C.T., Australia.
[3]Hydrological Sciences Branch, NASA Goddard Space Flight Center, Greenbelt, Maryland, USA.

Published in 2007 by American Geophysical Union.

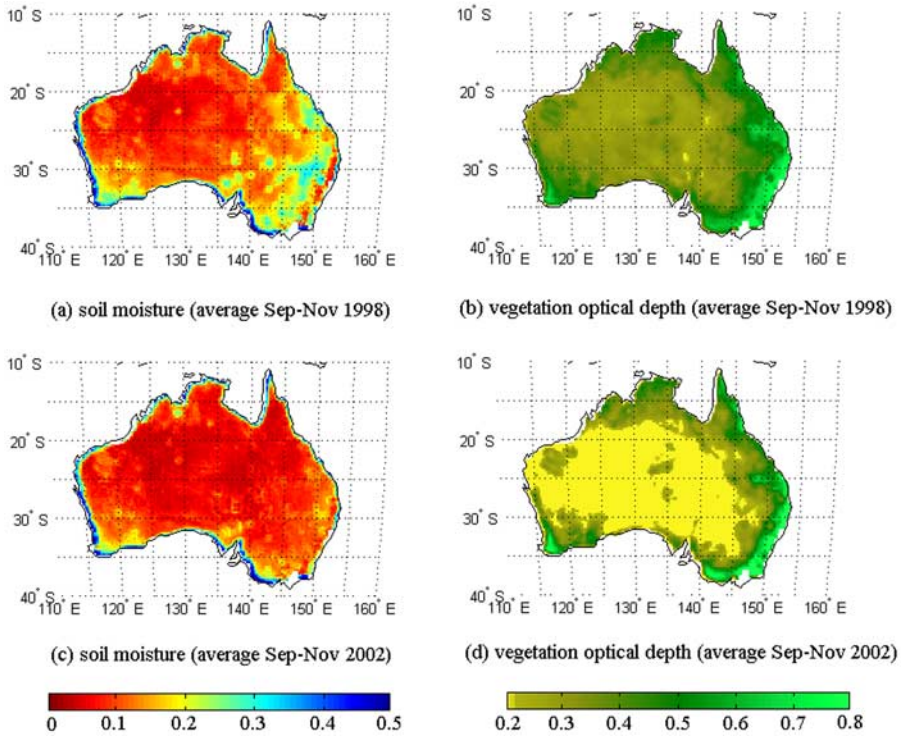

Figure 1. Average soil moisture (θ in m^3 m^{-3}) in top 1-cm of soil and vegetation optical depth (τ) for a wet spring (September–November 1998) and a dry spring (2002) across mainland Australia.

Meesters et al., 2005] and X-band brightness temperature. The retrieved soil moisture represents roughly the top 1-cm, because TMI with the low observing frequency of 10.7 GHz (X-band) has a source depth of about 1 cm. It has been evaluated against various observational and simulated datasets, generally with good results and with an absolute accuracy of ca. 0.06 m^3 m^{-3} [*Owe et al.*, 2001; *de Jeu and Owe*, 2003; *O'Neill et al.*, 2006; *Wagner et al.*, 2007].

[7] Vegetation optical depth (τ) is a dimensionless parameter that can be interpreted as being directly proportional to vegetation water content [*Jackson and O'Neill*, 1990; *Jackson and Schmugge*, 1991] and was derived according to *Meesters et al.* [2005].

[8] The retrieved soil moisture and vegetation optical depth data were resampled and aggregated into seasonal average 0.25° resolution images for December 1997 through December 2005 for mainland Australia. Two spring seasons - one wet, the other dry - are shown in Figure 1. Areas where observations are influenced by open water or snow are left white.

[9] The ocean circulation indicators used in this study were the Southern Oscillation Index (SOI), the North Atlantic Oscillation (NAO) and the Indian Ocean Dipole (IOD) Mode Index. The SOI is obtained from the Bureau of Meteorology of Australia (http://www.bom.gov.au/climate/current/soihtm1.shtml), IOD index from the Japan Agency for Marine-Earth Science and Technology (http://www.jamstec.go.jp/frsgc/research/d1/iod/) and NAO index from the National Oceanic and Atmospheric Administration (NOAA, ftp://ftp.cpc.ncep.noaa.gov/wd52dg/data/indices/tele_index.nh). The SOI used is the standardized anomaly of the mean sea level pressure difference between Tahiti and Darwin (Troup SOI) [*McBride and Nicholls*, 1983]. *Saji et al.* [1999] defined the IOD index as the sea surface temperature difference between the tropical western Indian Ocean (10°S–10°N, 50°E–70°E) and the tropical southeastern Indian Ocean (10°S–equator, 90°E–110°E). The NAO index is constructed by comparing daily 500 mb height anomalies over the Northern Hemisphere to monthly mean 500 mb air pressure height for 1950 through 2000 [*Barnston and Livezy*, 1987].

2.2. Methods

[10] The Empirical Orthogonal Function (EOF) analysis and rank correlation analysis were used in this study. The EOF analysis [*Bjornsson and Venegas*, 2000] produces a set of functions that represent various modes of oscillation dominating in a spatiotemporal data set, and the relative importance of each pattern in explaining observed variation across space. It has been applied to study correlation between Northern Hemisphere air temperature and satellite-derived greenness, and El Niño Southern Oscillation (ENSO) and Arctic Oscillation [*Buermann et al.*, 2003]. Here the EOF analysis was performed on seasonal averages of θ and τ, and Spearman's rank correlation coefficients were calculated between the first two EOFs of each observation and the SOI, IOD and NAO indicators.

[11] We used rank (non-parametric) correlation analysis to evaluate the strength of the correlation between the first two EOFs of θ and τ, and SOI, IOD and NAO indices for each of the four seasons. We also used this to map the

Table 1. Variance Explained by the First Four EOF Patterns in Soil Moisture and Vegetation Optical Depth for Four Seasons[a]

	EOF1, %	EOF2, %	EOF3, %	EOF4, %	Total, %
Spring θ	57	13	10	6	86
Spring τ	56	17	11	6	90
Summer θ	41	17	15	8	81
Summer τ	59	13	11	5	88
Autumn θ	59	16	7	6	88
Autumn τ	62	13	8	5	88
Winter θ	38	21	12	11	82
Winter τ	61	16	6	5	88

[a]Variance explained in percentage; soil moisture, θ; vegetation optical depth, τ.

correlation between spring θ with and SOI and IOD indices across Australia.

3. Results

[12] The variances explained by the first four EOFs for θ and τ of four seasons are listed in Table 1. Rank correlation coefficients between the leading two EOFs and SOI, IOD and NAO indices are listed in Figure 2. The respective EOFs for θ and τ are reasonably well correlated for most of the year, but in winter both τ-EOFs appear correlated to θ-EOF2 but not to θ-EOF1, and in summer the respective second EOFs are not correlated at all. In other words, the coupling between θ and τ appears strongest in spring and autumn, and least in winter.

[13] The θ-EOF1 for all seasons and τ-EOF1 for spring and autumn are moderately to strongly correlated to SOI. The strongest correlations (r^2 = 0.90) are for spring (Figure 2). Wet seasons correspond to higher than average SOI (1998–2001) and dry seasons to lower than average SOI (2002–2005) Figure 3.

Summer / Spring	θ EOF1	θ EOF2	τ EOF1	τ EOF2	SOI	IOD	NAO
θ EOF1		-	0.54[b]	-	0.69[b]	-	-
θ EOF2	-		-	-	-	-	-
τ EOF1	0.90[a]	-		-	0.48	0.38	-
τ EOF2	-	-	-		-	-	0.38
SOI	0.90[a]	-	0.90[a]	-		-	-
IOD	0.58[b]	-	0.41	-	0.48		-
NAO	-	-	-	-	-	-	

Winter / Autumn	θ EOF1	θ EOF2	τ EOF1	τ EOF2	SOI	IOD	NAO
θ EOF1		-	-	-	0.77[b]	-	0.48
θ EOF2	-		0.51[b]	0.51[b]	-	-	-
τ EOF1	0.73[b]	-		-	-	-	-
τ EOF2	-	0.77[b]	-		0.58[b]	-	-
SOI	0.69[b]	-	0.66[b]	-		-	-
IOD	0.41	-	-	-	0.50		-
NAO	-	-	-	-	-	-	

Figure 2. Rank (non-parametric) correlation coefficients (r^2) between the leading two EOF patterns of soil moisture (θ) and vegetation optical depth (τ) of the four seasons, and SOI, IOD, and NAO indices. Tables are split diagonally: all values for one season are in the bottom-left half; all values for another season in the top-right half. Suffixes [a] and [b] indicate correlation significance at 0.01 and 0.05 level, respectively; the remaining values are significant at 0.10 (one-tailed test).

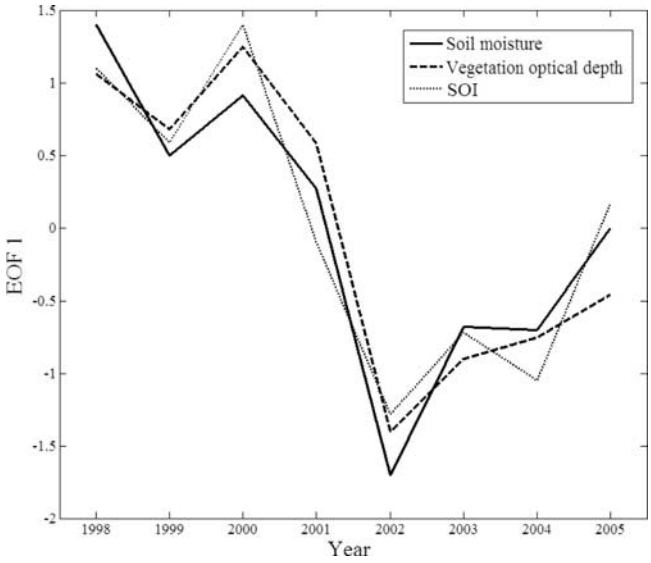

Figure 3. Normalized time series of the first EOFs of spring (September–November) θ and τ and the SOI index for the period 1998–2005. Data shown as anomalies from the mean normalized by standard deviation.

[14] In addition, θ-EOF1 is significantly correlated to IOD in spring. The coefficient of correlation is greater than that between SOI and IOD, which suggests that this is not merely a spurious correlation. While not significant at 0.05 level, the correlation between θ-EOF1 and NAO in winter is still relatively high (r^2 = 0.48).

[15] The spatial structures of the first EOFs for spring θ and τ show that these signals are strongest in eastern Australia, in particular in eastern Queensland and the eastern Murray-Darling Basin (Figure 4). The strength between θ and SOI and IOD for spring only is shown in Figures 5 (top) and 5 (bottom), respectively.

4. Discussion and Conclusions

[16] For the period 1998 through 2005, we found a strong correlation between seasonal soil and vegetation moisture content derived from passive microwave observations and SOI, particularly for eastern Australia in spring, and also for autumn and summer. In addition, we found a signal relating both θ and τ to IOD in spring and the strongest correlation between θ and τ in spring and autumn. For most of the continent, these seasons coincide with the transition between dry and wet season (or vice versa) and associated with this the greening and senescence of annual vegetation. Delays in these transitions associated with oceanic circulation patterns may explain the stronger correlation. The influence of ENSO on rainfall has been documented [e.g., *McBride and Nicholls*, 1983; *Allan et al.*, 1996], as has that of IOD [*Simmonds*, 1990; *Drosdowsky*, 2002; *Saji et al.*, 1999]. The spatial patterns of ENSO influence on soil moisture agree well with those found in rainfall (cf. maps based

on interpolated station rainfall on http://www.bom.gov.au/climate/enso/ninocomp.shtml). Our results provide further evidence that ENSO, and to a lesser extent IOD, can also be linked to the drought conditions experienced since 2000. It shows that the ENSO/IOD influence on rainfall is also evident in the soil moisture and vegetation record.

[17] Without using station rainfall records, we were able to directly delineate regions experiencing the strongest influence of ENSO during the period analyzed. The most affected regions are in the Murray-Darling Basin and Queensland; both are important agricultural regions.

[18] It is noted that the time series analyzed covers only the moderate 2002 El Niño event (although spring 2004 could be considered a very weak event when using a less strict definition). Development of a longer time series of global data of soil moisture, vegetation optical depth and surface temperature compiled from different passive microwave observation sources should help to identify whether the high correlations found in this study are maintained and to better understand seasonal and inter-annual variations in climate associated with ocean circulation patterns.

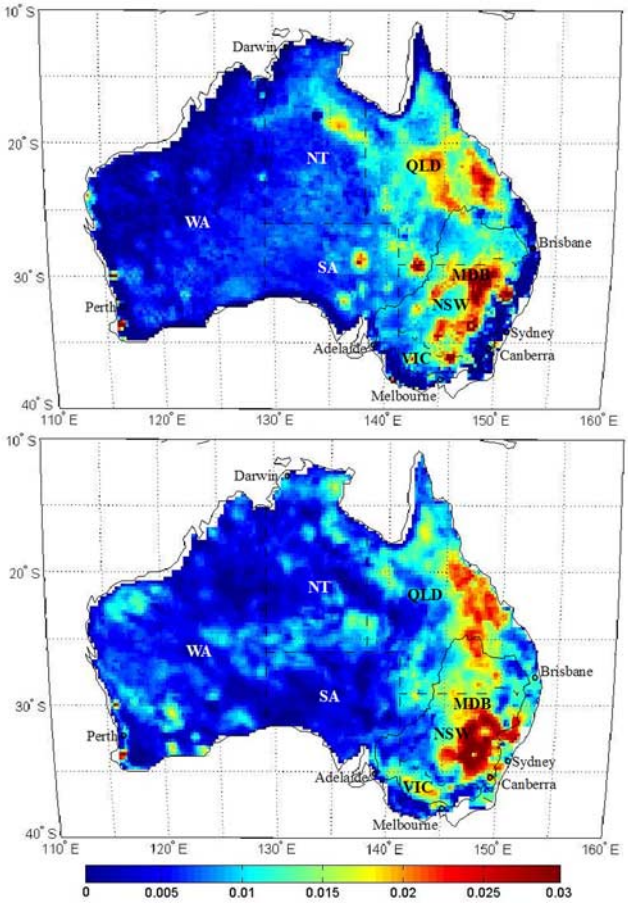

Figure 4. The first EOF pattern in spring (September to November) for (top) soil moisture (θ), explaining 57% of total variation; and (bottom) vegetation optical depth (τ), explaining 56% of total variation. WA, Western Australia; NT, Northern Territory; QLD, Queensland; SA, South Australia; NSW, New South Wales; VIC, Victoria; MDB, Murray Darling Basin.

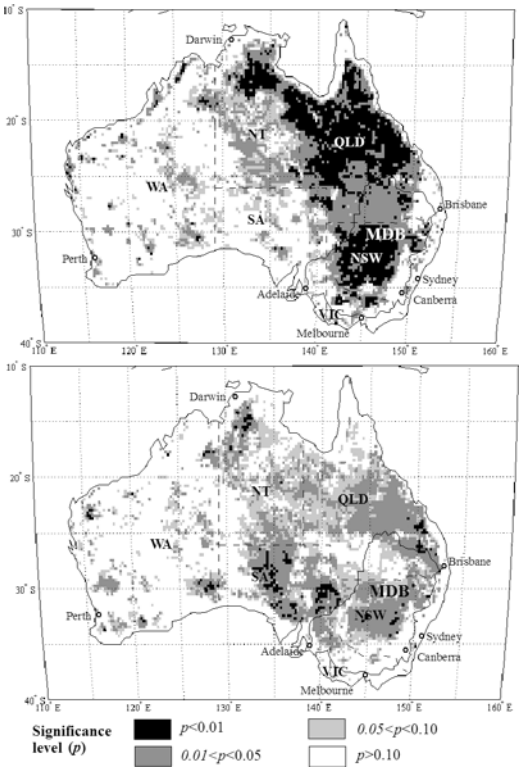

Figure 5. Spatial patterns in the strength of the connection between spring values of (top) θ and SOI; and (bottom) θ and IOD, calculated as the statistical significance of the ranked correlation (one-tailed test).

References

Abram, N. J., M. K. Gagan, Z. Liu, W. S. Hantoro, M. T. McCulloch, and B. W. Suwargadi (2007), Seasonal characteristics of the Indian Ocean Dipole during the Holocene epoch, *Nature*, *445*, 299–302, doi:10.1038/nature05477.

Allan, R., J. Lindesay, and D. E. Parker (1996), *El Niño Southern Oscillation and Climatic Variability*, 416 pp., CSIRO, Melbourne, Victoria, Australia.

Ashok, K., Z. Guan, and T. Yamagata (2003), Influence of the Indian Ocean Dipole on the Australian winter rainfall, *Geophys. Res. Lett.*, *30*(15), 1821, doi:10.1029/2003GL017926.

Barnston, A. G., and R. E. Livezy (1987), Classification, seasonality and persistence of low-frequency atmospheric circulation patterns, *Mon. Weather Rev.*, *115*, 1083–1126.

Beeton, R. J. S., K. I. Buckley, G. J. Jones, D. Morgan, R. E. Reichelt, and T. Dennis (2006), Australia state of the environment 2006, independent report to the Australian Government Minister for the Environment and Heritage, Dep. of the Environ. and Heritage, Canberra, A.C.T., Australia.

Bjornsson, H., and S. A. Venegas (2000), A manual for EOF and SVD analyses of climatic data, 53 pp., McGill Univ., Montreal, Que., Canada.

Buermann, W., B. Anderson, C. J. Tucker, R. E. Dickinson, W. Lucht, C. S. Potter, and R. B. Myneni (2003), Interannual covariability in Northern Hemisphere air temperatures and greenness associated with El Niño-Southern Oscillation and the Arctic Oscillation, *J. Geophys. Res.*, *108*(D13), 4396, doi:10.1029/2002JD002630.

Campbell, J. B. (2002), *Introduction to Remote Sensing*, 3rd ed., Guilford Press, New York.

Choudhury, B. J. (1993), Desertification, in *Atlas of Satellite Observations Related to Global Change*, edited by R. J. Gurney, J. L. Foster, and C. L. Parkinson, pp. 313–326, Cambridge Univ. Press, New York.

de Jeu, R. A. M., and M. Owe (2003), Further validation of a new methodology for surface moisture and vegetation optical depth retrieval, *Int. J. Remote Sens.*, *24*, 4559–4578.

Drosdowsky, W. (2002), SST phases and Australian rainfall, *Aust. Meteorol. Mag.*, *51*, 1–12.

Fensholt, R., and I. Sandholt (2003), Derivation of a shortwave infrared water stress index from MODIS near- and shortwave infrared data in a semiarid environment, *Remote Sens. Environ.*, *87*, 111–121.

Horridge, M., J. Madden, and G. Wittwer (2005), The impact of the 2002–2003 drought on Australia, *J. Policy Model.*, *27*, 285–308, doi:10.1016/j.jpolmod.2005.01.008.

Jackson, T. J., and P. E. O'Neill (1990), Attenuation of soil microwave emission by corn and soybeans at 1.4 and 5 GHz, *IEEE Trans. Geosci. Remote Sens.*, *28*, 978–980.

Jackson, T. J., and T. J. Schmugge (1991), Vegetation effects on the microwave emission from soils, *Remote Sens. Environ.*, *36*, 203–212.

Kummerow, C., W. Barnes, T. Kozu, J. Shiue, and J. Simpson (1998), The Tropical Rainfall Measuring Mission (TRMM) sensor package, *J. Atmos. Oceanic Technol.*, *15*, 809–817.

McBride, J. L., and N. Nicholls (1983), Seasonal relationships between Australian rainfall and the Southern Oscillation, *Mon. Weather Rev.*, *111*, 1998–2004.

McVicar, T. R., and D. L. B. Jupp (1998), The current and potential operational uses of remote sensing to aid decisions on drought exceptional circumstances in Australia: A review, *Agric. Syst.*, *79*(2), 399–468.

McVicar, T. R., and D. L. B. Jupp (2002), Using covariates to spatially interpolate moisture availability in the Murray-Darling Basin: A novel use of remotely sensed data, *Remote Sens. Environ.*, *79*, 199–212.

Meesters, A. G. C. A., R. A. M. de Jeu, and M. Owe (2005), Analytical derivation of the vegetation optical depth from the microwave polarization difference index, *IEEE Trans. Geosci. Remote Sens.*, *2*, 121–123.

Murphy, F., and J. Ribbe (2004), Variability of southeastern Queensland rainfall and climate indices, *Int. J. Climatol.*, *24*, 703–721.

Nicholls, N. (2004), The changing nature of Australian droughts, *Clim. Change*, *63*, 323–336.

O'Neill, P. E., E. G. Njoku, J. Shi, E. F. Wood, M. Owe, and B. Gouweleeuw (2006), Hydros soil moisture retrieval algorithms: Status and relevance to future missions, paper presented at International Geoscience and Remote Sensing Symposium, IEEE, Denver, Colo., 31 July–4 Aug.

Owe, M., R. A. M. de Jeu, and J. P. Walker (2001), A methodology for surface soil moisture and vegetation optical depth retrieval using the microwave polarization difference index, *IEEE Trans. Geosci. Remote Sens.*, *39*, 1643–1654, doi:10.1109/36.942542.

Owe, M., R. A. M. de Jeu, and T. Holmes (2007), Multi-sensor historical climatology of satellite-derived global land surface moisture, *J. Geophys. Res.*, doi:10.1029/2007JF000769, in press.

Saji, N. H., B. N. Goswami, P. N. Vinayachandran, and T. Yamagata (1999), A dipole mode in the tropical Indian Ocean, *Nature*, *401*, 360–363.

Simmonds, I. (1990), A modeling study of winter circulation and precipitation anomalies associated with Australian region ocean temperatures, *Aust. Meteorol. Mag.*, *38*, 151–161.

Streten, N. A. (1981), Southern hemisphere sea surface temperature variability and apparent associations with Australian rainfall, *J. Geophys. Res.*, *86*, 485–497.

Streten, N. A. (1983), Extreme distributions of Australian rainfall in relation to sea surface temperature, *J. Climatol.*, *3*, 143–153.

Wagner, W., V. Naeimi, K. Scipal, R. de Jeu, and J. M. Fernandez (2007), Soil moisture from operational meteorological satellites, *Hydrogeol. J.*, *15*, 121–131, doi:10.1007/s10040-006-0104-6.

R. A. M. de Jeu, Department of Hydrology and Geo-Environmental Sciences, Faculty of Earth and Life Sciences, Vrije Universiteit Amsterdam, De Boelelaan 1085, Amsterdam, 1081 HV Netherlands.

Y. Liu and A. I. J. M. van Dijk, Black Mountain Laboratory, CSIRO Land and Water, G.P.O. Box 1666, Canberra, A.C.T. 2601, Australia. (yiliu001@gmail.com)

M. Owe, Hydrological Sciences Branch Mail Code 614.3, NASA Goddard Space Flight Center, Greenbelt, MD 20771, USA.